INSTITUTE FOR FUSION STUDIES

DOE/ET-53088-491 IFSR #491

Magnetic Interchange Instability of Accretion Disks

M. KAISIG, T. TAJIMA, and R.V.E. LOVELACE*
Institute for Fusion Studies
The University of Texas at Austin
Austin, Texas 78712

March 1991

*permanent address: Dept. of Applied Physics, Cornell University, Ithaca, NY 14853

THE UNIVERSITY OF TEXAS

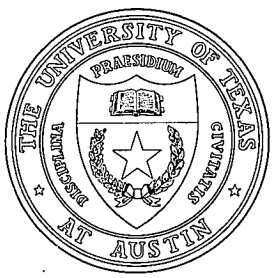

AUSTIN

Magnetic Interchange Instability of Accretion Disks

M. Kaisig,[1] T. Tajima,[1] and R.V.E. Lovelace[1,2]

February 8, 1991

[1] Department of Physics and Institute for Fusion Studies, University of Texas, Austin, TX 78712

[2] Department of Applied Physics, and Department of Astronomy, Cornell University, Ithaca, New York 14853

Headings: Accretion Disks, Magnetohydrodynamics, Instabilities

Abstract

A study is made of the nonlinear evolution of the magnetic interchange or buoyancy instability of a differentially rotating disk threaded by an ordered vertical magnetic field. As a model for the disk we consider a two-dimensional ideal fluid in the equatorial plane of a central mass in the corotating frame of reference. We use a local approximation of a shearing sheet and study the evolution numerically by solving the equations of ideal magnetohydrodynamics.

If the rotation rate of the disk is Keplerian, the disk is found to be stable. If the vertical magnetic field is sufficiently strong, and the field strength decreases with distance from the central object, and thus the rotation of the disk deviates from Keplerian, we find that an instability develops. The magnetic flux and disk matter expand outwards in certain ranges of azimuth while disk matter with less magnetic flux move inward over the remaining range of azimuth, showing a characteristic development of an interchange instability. Saturation and eventually decay occurs when the field enters the outer Keplerian part of the disk. The growth rate ω_i in the initial, linear regime depends on the azimuthal wavenumber k of the initial perturbation as $\omega_i \sim k^{1/2}$. The growth rate decreases as $\beta = 4\pi p/B^2$ increases and vanishes for $\beta > 5$.

When a slow but steady supply of vertical magnetic field is present in the accretion flow, the magnetic perturbation persists and gives rise to a steady-state disk configuration in which there is an outward angular momentum transport which corresponds to a dimensionless viscosity (Shakura-Sunyaev) parameter of $\alpha \sim 0.1$.

I. Introduction

Accretion disks are thought to have an important role in many astronomical objects, ranging from X-ray binary sources to the nuclei of active galaxies and quasars.

The release of gravitational energy by the spiraling infall of ionized gas in a disk requires the simultaneous outflow of angular momentum, which in the standard model of Shakura and Sunyaev(1973) occurs as a result of a turbulent viscous stress. The origin of the turbulence and the value of the effective viscosity remains a fundamental unsolved problem. In two and three dimensional hydrodynamical simulations of the flow in thin accretion disks, no significant turblence was found (Kaisig 1989; Kaisig and Spruit 1991).

The possible importance of small-scale magnetic fields in producing a viscous stress has been recognized and studied by many authors (for example, Lynden-Bell 1969; Shakura and Sunyaev 1973; Eardley and Lightman 1975; and Coroniti 1981). Much less attention has been given to the importance of a large-scale, well-ordered magnetic field for angular momentum transport. A well-ordered magnetic field is thought to also be important for the formation of jets and winds (Bandford and Payne 1982; Lovelace, Wang, and Sulkanen 1987; Lovelace, Berk, and Contopoulos 1991; Uchida et al. 1985). The quasi-periodic pulsations of dwarf novae have been related to the azimuthal structure and reconnection of large-scale magnetic fields (Tajima and Gilden 1987).

The present work considers the situation of an accretion disk formed from the ionized gas of a large, slowly-rotating cloud which is threaded by a weak, but well-ordered magnetic field that has a component parallel to the cloud's rotation axis. That is, the field is assumed to have a vertical component. This weak cloud field could arrise from dynamo activity in a turbulent rotating cloud. The accretion flow acts to drag this field inward towards the central accreting object. The strength of the magnetic field is determined, in the absence of instabilities, by the "frozen-in" flux condition so that $B_z(r,t)$ is proportional to the surface density of a mass element of the disk. The B_z flux will accumulate in the inner region of the disk and, in the absence of instabilities, it will become dynamically important. A magnetic field of

strength $B_z^2/8\pi \sim (\rho v_\phi^2)_{disk}$ in the inner part of the disk will cause the disk matter to rotate at a substantially sub-Keplerian rate (Lovelace et al. 1986).

This paper discusses results from a computer simulation study of the non-linear magnetohydrodynamics of an accretion disk threaded by a strong vertical magnetic field. We find that for conditions of physical interest there is a strong interchange (or Rayleigh-Taylor) instability involving a finite azimuthal wavenumber. The condition for the onset of this instability was discussed earlier by Lovelace and Scott(1981). The non-linear phase of the instability involves the radial exchange of high flux, high surface density disk matter from small radial distances (over one range of azimuth) with a low flux, low surface density matter at large radial distances (over the remaining range of azimuth). It appears that the non-linear instability can provide significant outward radial transport of magnetic flux and angular momentum.

Section II gives the basic equations and discusses the assumptions made for the numerical simulations. Section III present the numerical results, and §IV discusses a possible steady state of the non-linear instability. Section V gives the conclusions of this work.

II. Basic equations and numerical methods

a) Assumptions and Basic Equations

As a model for the accretion disk we consider a two-dimensional fluid in the equatorial plane perpendicular to the rotation axis. We adopt the local approximation of a shearing sheet (Goldreich and Lynden-Bell 1965; Goldreich and Tremain 1978; Narayan et al. 1987; Kaisig 1989), which represents a small "patch" of the disk. For our numerical simulations the following additional assumptions are made: (1) the medium is an ideal gas, (2) the gas obeys the isentropic relation $p \propto \rho^\gamma$, where $\gamma = const.$, where p is the pressure, and where ρ is the surface mass density, (3) the magnetic field is frozen in the gas. Cartesian coordinates (x, y, z) are adopted with

the z-direction parallel to the rotation axis, with x in the radial direction, and with y in the azimuthal direction. It is assumed that the evolution is approximately two-dimensional with $V_z = 0, \partial/\partial z = 0$, and ${B_z}^2 \gg {B_x}^2$ or ${B_y}^2$. In a frame of reference rotating with the fluid at angular velocity Ω_0, the basic equations are:

$$\frac{\partial \rho}{\partial t} + \frac{\partial}{\partial x}(\rho V_x) + \frac{\partial}{\partial y}(\rho V_y) = 0, \tag{1}$$

$$\frac{\partial}{\partial t}(\rho V_x) + \frac{\partial}{\partial x}\left[\rho {V_x}^2 + p + \frac{{B_z}^2}{8\pi}\right] + \frac{\partial}{\partial y}(\rho V_x V_y) = (2\rho V_y + 3\rho x), \tag{2}$$

$$\frac{\partial}{\partial t}(\rho V_y) + \frac{\partial}{\partial x}(\rho V_y V_x) + \frac{\partial}{\partial y}\left(\rho {V_y}^2 + p + \frac{{B_z}^2}{8\pi}\right) = -2\rho V_x, \tag{3}$$

$$\frac{\partial B_z}{\partial t} + \frac{\partial}{\partial x}(V_x B_z) + \frac{\partial}{\partial y}(V_y B_z) = 0, \tag{4}$$

$$\begin{aligned} &\frac{\partial}{\partial t}\left[\frac{p}{\gamma - 1} + \frac{1}{2}\rho({V_x}^2 + {V_y}^2 + {V_z}^2) + \frac{1}{8\pi}({B_z}^2)\right] \\ &+\frac{\partial}{\partial x}\left[\frac{\gamma}{\gamma - 1} p V_x + \frac{1}{2}\rho V_x({V_x}^2 + {V_y}^2) + \frac{B_z}{4\pi}(V_x B_z)\right] \\ &+\frac{\partial}{\partial y}\left[\frac{\gamma}{\gamma - 1} p V_y + \frac{1}{2}\rho V_y({V_x}^2 + {V_y}^2) + \frac{B_z}{4\pi}(V_y B_z)\right] \\ &-3\rho x V_x = 0, \end{aligned} \tag{5}$$

Equation (1) is the continuity equation; equations (2) and (3) are the radial and azimuthal components of the Euler equation, respectively; equation (4) is the condition for frozen in flux; and equation (5) is for energy conservation. The first term on the right-hand-side of equations (2) and (3) represents the Coriolis force. The second term on the right-hand-side of equation (3) describes the difference between the gravitational and centrifugal forces in the corotating frame of reference.

Equations (1) - (5) are made dimensionless by using the rotation period $1/\Omega_0$ as a reference time scale, $h_0 = C_s/\Omega_0$ as a reference length scale, where C_s is the isothermal speed of sound, and ρ_0 the surface mass density at $(x = 0)$. Notice that h_0 is of the order of the vertical thickness of the disk.

b) Initial conditions

The initial equilibrium is shown in Figure 2. Specifically, we consider an isothermal plasma with temperature $T = 1$ in dimensionless units, and an initial magnetic field $\vec{\mathbf{B}} = (0, 0, B_z(x))$, where $|B_z(x)|$ decreases with distance x so that in the outer part of the disk the B-field is weak. The variation of the equilibrium magnetic field strength $B_z(x)$ is given by

$$B_z(x) = [8\pi p(x)/\beta(x)]^{1/2}, \tag{6}$$

where

$$\beta(x) = \beta_0 / f(x), \tag{7}$$

$$f(x) = \frac{1}{2} \cdot \left[1 - tanh\left(\frac{x - x_0}{w_0}\right)\right], \tag{8}$$

and where β_0 is the ratio of the gas pressure to magnetic pressure at the inner edge of the shearing sheet, x_0 determines the radial extent of the magnetic field, and w_0 is the width of the transition region between the magnetized and unmagnetized disk. In all our calculations we assume that the initial magnetic field is localized in the inner part of the disk with $x_0 = X_{min} + 2.0$ and $w_0 = 0.5$.

The initial density and pressure distributions are numerically calculated using equations (6) and (7) and the equation for the radial force balance

$$\frac{d}{dx}\left[p(x) + \frac{{B_z}^2(x)}{8\pi}\right] - (2\rho V_y + 3\rho x) = 0. \tag{9}$$

Notice that as a result of the magnetic pressure, the inner part of the disk rotates more slowly than it would in a Keplerian disk. Thus the disk matter is partially supported by the magnetic field. This situation is possibly unstable to the interchange instability.

We assume an initial azimuthal velocity profile

$$V_y(x) = -q \cdot x, \tag{10}$$

in the corotating frame, where the shear rate $q = 2$ corresponds to a constant angular momentum disk, $q = 1.5$ to a thin Keplerian disk and $q = 1$ to a system with constant circular velocity.

On the initial equilibrium we impose a small radial velocity perturbation of the form

$$\delta V_x(x, y) = A \cdot f(x) cos(k\frac{y}{\lambda}), \tag{11}$$

where $k = 2\pi/\lambda$, with λ the azimuthal wavelength, where A is the amplitude of the perturbation, and where $f(x)$ is given in equation (8).

c) Boundary conditions

We take periodic boundaries at $y = 0$ and $y = Y_{max}$, and rigid boundaries for $x = X_{min}$ and $x = X_{max}$. We have also simulated the case with a free boundary at $x = X_{max}$. As long as we study the onset and the early evolution of the instability, the effect of the free boundary is small (§III). For the long term evolution of the interchange mode in the case of a steady magnetic flux supply, studied in §IV, the outer free boundary is essential.

In a typical run the mesh sizes are $\Delta x = 0.1$ and $\Delta y = 0.4$. The total number of mesh points is $(N_x \times N_y) = (103 \times 53)$, the total area is $|(X_{max} - X_{min}) \times Y_{max}| = |5 \times 40|$ with $X_{min} = -2.5$ and $X_{max} = 2.5$ in units of the characteristic length scale h_0.

d) Numerical method

Equations (1) - (5) are solved numerically by using a modified Lax-Wendroff scheme (Rubin and Burstein 1967) with an artificial viscosity (Richtmyer and Morton 1967). The tests and accuracy of such a MHD code have been described by Shibata (1983), Shibata and Uchida (1985), Matsumoto *et al.* (1988), Umemura it et al. (1988), and Tajima (1989).

III. Onset and early evolution of the instability

a) Overall Evolution

We first present results for a representative case which shows the basic characteristics of the nonlinear evolution of the interchange instability. The parameters of this simulation are: $\beta_0 = 0.2$, $A = 0.05$, and $\lambda = 10$. We assume Keplerian rotation ($q = 1.5$) in the outer, unmagnetized part of the disk ($x \geq 0$), and a smaller shear rate ($q = 0.8$) in the inner part ($x < 0$).

Figure 1 shows the time variations of the contour lines of the magnetic field B_z, the surface density distribution ($log\rho$), and the velocity perturbations ($\delta V_x, \delta V_y$), where

$$\delta V_y = V_y - < V_y(x,y) >_y \qquad (12)$$

is the azimuthal velocity relative to the mean background flow.

As the instability develops, the magnetic flux expands outwards. In the case of a non-shearing medium, the instability is responsible for the formation of mushroom shaped structures (Cattaneo and Hughes 1988). In the present situation where the interchange mode occurs in a differentially rotating disk, magnetic loops form which are distorted by the strong shear. The plasma slides down the expanding loop along the lines of constant B-field. Shock waves form in the downflow. Spiral shaped shock fronts form in the outer part of the disk, as can be seen in the velocity and density plots at $t = 20$. The initial instability of the magnetic field gives rise to strong shearing motions, thereby exciting secondary Kelvin-Helmholtz instability. The subsequent motions are determined primarily by the strong interactions between vortices which are responsible for the rapid disruption of the magnetic structures in the later stage and the final trend to an axisymmetrix configuration.

Stabilization of the regions of expanding magnetic flux occurs when the field enters the part of the disk which rotates with Keplerian velocity ($x \geq 0$). In the final state ($t = 38$) the magnetic field and density distributions are nearly axisymmetric.

Figure 2 shows the azimuthally averaged radial distributions of the azimuthal velocity V_y, total pressure P_{tot}, thermal pressure p, magnetic pressure p_{mag}, surface density ρ, and the resulting angular momentum transport in the initial and final states. The angular momentum transport is measured by the dimensionless parameter α of Shakura and Sunyaev(1973),

$$t_{r\phi} = \alpha \cdot p, \tag{13}$$

where $t_{r\phi}$ is the radial flux of angular momentum. Averaged over the azimuthal direction, the $\alpha-$ parameter can be determined from our simulations,

$$\alpha(x) = < \frac{1}{p} \cdot (\rho V_x V_y) >_y . \tag{14}$$

Initially, the inner part of the disk ($x \leq 0$) rotates slower than Keplerian (Fig. 2a). The slower rotation is balanced by the gradient of the magnetic pressure. The magnetic flux is initially concentrated in the inner region of the disk (Fig. 2d). In the outer part of the disk ($x \geq 0$) the pressure is constant, and the rotation rate is Keplerian. In the isothermal case considered here, the gas pressure gives rise to a density distribution as shown in Fig. 2e. The important affect of the magnetic field is that it acts to support matter against gravity. As mentioned above, this situation where a dense fluid is supported by a lighter fluid gives rise to the interchange mode.

In the course of the evolution, the average azimuthal velocity in the inner region of the disk approaches the Keplerian rotation rate. For the final state calculated ($t = 38$) the azimuthal velocity profile in the inner region of the disk ($x \leq 0$) is given approximately by a shear rate of $q = 1.3$ compared to $q = 0.8$ initially. In the outer region of the disk $q = 1.5$, which is the Keplerian value.

In Fig. 2f we show the angular momentum transport as measured by the $\alpha-$parameter. The high $\alpha-$value at $t = 10$ corresponds to the radial expansion of the magnetic flux within the inner part of the disk. Finally, as the instability saturates the $\alpha-$ parameter drastically decreases.

The instability is finally stabilized by the outer Keplerian region of the disk. The magnetic field penetrates only to a small extent into the outer region of the disk. Thus, in the course of the evolution, the instability leads to a redistribution of matter and angular momentum in such a way that the final distribution is similar to the case of a Keplerian disk, and the net angular momentum transport tends to be zero.

Figure 3 displays the time variation of magnetic, gravitational, thermal, kinetic and total energies in the system, where all the energies are normalized to their initial values. The evolution is gradual in the initial, linear phase. After this initial period, the magnetic field quickly expands outwards and reduces the magnetic field energy. Most of the released energy is converted into kinetic energy, and as shown in Fig. 2a, this goes mostly into rotational energy of the initially non-Keplerian disk. By the time $t \sim 15$ (Fig. 3) the kinetic energy ceases to grow. At this stage there is a change in the dynamics. Initially the dynamics is controlled by the expansion of the magnetic flux, the formation of loop-shaped structures, the downflow of material along the lines of constant B-field, and the creation of regions of strong vorticity. In the subsequent evolution the system is controlled by the strong interaction of the vortices.

In the final state the gravitational energy is slightly higher and the thermal energy slightly lower than in their initial states. The total energy in the simulation is conserved within 2% of its initial value.

b) Dependence on the wavelength, plasma β and shear rate

We have studied the time dependence of the kinetic energy of the perturbations for different wavelengths of the initial disturbances and for different plasma β and shear rates of the inital model.

Figure 4 shows the evolution resulting from our numerical simulations with initial wavenumbers $k = 1$, $k = 4$, and $k = 6$ as a function of $k^{1/2} \cdot t$. The case $k = 1$ discussed

in Section IIa, corresponds to a wavelength of $\lambda = 10h_0$. The results of the numerical simulations show that the growth rate ω_i depends on the azimuthal wavenumber as $\omega_i \sim k^{1/2}$ in the early stage of the evolution, as expected from the linear theory of the interchange or Rayleigh-Taylor instability. In the non-linear regime the growth rates strongly increase before stabilization sets in at $(k^{1/2} \cdot t) \approx 8$. The final state is independent of the wavelength of the initial perturbation and shows in all cases the same basic characteristics described in Section IIa.

In Fig. 5 we display the time variations of the perturbation energy for different values of β of the initial configuration. We performed the simulations with a resolution of $\Delta x = 0.1$ and $\Delta y = 0.4$. For the cases of $\beta_0 = 0.2$ and $\beta_0 = 5.0$ we also studied the evolution with a grid size of $\Delta x = 0.033$ and $\Delta y = 0.4$. Figure 5 shows the dependence of the growth rate on $\beta = 4\pi p/B^2$. Higher spatial resolution does not influence the early stages of evolution but becomes significant in the later phase. In the later stage the higher resolution is more important in the case of large β_0, where it indicates slower growth rates. For $\beta_0 \geq 5.0$ we find no evidence for the interchange instability.

Figure 6 shows the dependence of the perturbation energy on the initial shear of the azimuthal velocity profile in the inner part of the disk as determined by equation (10). The value $q = 0.8$ corresponds to the case studied in Section IIa with $\beta_0 = 0.2$, $\Delta x = 0.1$, $\Delta y = 0.4$, and $A = 0.05$. The growth rates decrease as the shear rate approaches $q = 1.5$ which corresponds to Keplerian rotation.

The main result of this part of the investigation is that the interchange instability saturates when the magnetic flux expands outwards into the outer part of the disk which rotates with Keplerian velocity. This stabilization might be removed if account is taken of a steady maintenance of magnetic field by the accretion flow. In the next section we address this problem.

IV. Long term evolution with a steady state magnetic field

Here we consider the situation where the magnetic flux in the inner region of the disk is continuously maintained by accretion. Thus, in our numerical simulations, we consider the situation where the magnetic field strength at the inner boundary is constant in time.

Furthermore, in this part of our investigation we assume an outer free boundary across which plasma can freely flow. This enables us to study the long term evolution of the interchange mode in the differentially rotating disk. The numerical representation of a free boundary is difficult. The choice of vanishing derivatives at the boundary leads in general to the partial reflection of hydromagnetic waves. In order to reduce the amplitude of reflected waves we include a wave absorbing zone just outside the physical system according to the prescription of Sato and Hayashi(1979). At the outermost boundary of the absorbing zone we require that the devivatives vanish.

We assume the same initial parameters used for the case shown in Fig. 1, where there was no maintenance of the magnetic field: $\beta_0 = 0.2$, $A = 0.05$, $\lambda = 10$, $q = 1.5$ in the outer, initially unmagnetized part of the disk, and $q = 0.8$ in the inner part.

Figure 7 shows the time dependence of the contour lines of the constant line magnetic field B_z, the density distribution ($\log \rho$) and the velocity perturbation $(\delta V_x, \delta V_y)$. Up to $t \sim 11$ the evolution is very similar to the case studied in section III. The magnetic flux again expands radially outwards in the form of loop like structures, vortices form and interact, and again there is downflow along the lines of constant $|B|$ and the formation of shocks. The important difference is that in the present case of a steady magnetic field at the inner edge of the disk, the expanding flux is not stabilized in the outer Keplerian part of the disk but continues spreading outwards.

After $t \sim 20$ the disk reaches a steady state in the sense that the azimuthally averaged quantities remain approximately constant (see Fig. 8 below). However, the disk is in a turbulent state. Figure 8 shows radial distributions of different azimuthally averaged quantities, including the dimensionless viscosity parameter α. As the instability develops and the magnetic flux expands outwards the disk deviates more and more from Keplerian rotation. In the final, steady state, the plasma rotates at a sub-Keplerian rate for all x (Fig. 8a). The radial transport of angular momentum transport as measured by α rises to 0.4 in the early evolution of the instability. In the final steady state (Fig. 8f), we find $\alpha \sim 0.1$.

The main new aspect of the case studied here is that stabilization of the interchange mode does not occur. In the saturated state, the disk has steady outward radial transport of both magnetic flux and angular momentum.

V. Summary and Discussion

We have presented results of numerical simulations of the nonlinear evolution of the magnetic interchange instability of an accretion disk threaded by a vertical magnetic field $B_z(r)$, which decreases with r. The important results of our investigation can be summarized as follows. As the interchange instability develops the magnetic field expands radially outwards. In the initial linear regime, the growth rate ω_i depends on the azimuthal wavenumber k as $\omega_i \sim k^{1/2}$. The growth rate of the instability decreases as $\beta = 4\pi p/B^2$ increases and there is no detectable growth rate for $\beta > 5$.

In accretion disks, magnetic field is continously advected inwards by the accretion flow. We take this into account by studying the case where the magnetic field is constant at the inner radial boundary of our simulation zone. We find that instability developes rapidly and approaches a saturated state in which there is a steady outward radial transport of both magnetic flux and angular momentum. The magnetic

field remains in a structured, turbulent configuration and thus acts to give efficient transport for $\beta < 1.0$. The final, steady state value of the dimensionless viscosity parameter is found from our simulations to be $\alpha \sim 0.1$. This value of α is of the order of the value suggested by observations (Pringle 1981; Verbunt 1981).

Therefore, the present process provides a possible mechanism for the anomalous viscosity in accretion disks for low β disks. However, this process is unable to give rise to a significant anomalous viscosity for high β disks. This demarcation of two kinds of disks is interesting, as a similar categorization was found due to the buoyancy instability in the vertical direction in an earlier work (Shibata et al. (1990), in which the azimuthal dynamics was neglected. In the present work, on the other hand we neglected the vertical dynamics.

The computations were performed on the Cray X-MP/24 and the Cray Y-MP8/864 at the Computer Center of the University of Texas at Austin. This work was supported by the National Science Foundation grant ATM88-11128, and US Department of Energy DE-FG05-80ET53088. One of the authors (R.L.) thanks the Guggenheim Foundation for fellowship support, David Baldwin for hospitality and support at the Institute for Fusion Studies at the University of Texas at Austin, and NASA for support from the Origins of the Solar System, grant NAGW 2293.

References

Blandford, R.D., and Payne, D.G. 1982, *Monthly Notices Roy. Astron. Soc.*, **199**, 883.

Cattaneo, F., and Hughes, D.W. 1988, J. Fluid Mech., **196**, 323.

Coroniti, F.V. 1981 *Astrophys. J.*,**244**, 587.

Eardley, D.M., and Lightman, A.P. 1975 *Astrophys. J.*,**200**, 187.

Goldreich, P., and Lynden-Bell, D. 1965, *Monthly Notices Roy. Astron. Soc.*, **130**, 125.

Goldreich, P., and Tremaine, S. 1978 *Astrophys. J.*,**222**, 850.

Kaisig, M. 1989, *Astron. Astrophys.*,**218**, 89.

Kaisig, M. and Spruit, H.C. 1991, in preparation.

Lovelace, R.V.E., and Scott, H.A., in Proc. of International School and Workshop on Plasma Astrophysics,1981, European Space Agency Publication ESA SP-161, p.215.

Lovelace, R.V.E., Mehanian, C., Mobarry, C.M., and Sulkanen, M.E. 1986, Astrophys. J. Suppl., **62**, 1.

Lovelace, R.V.E., Wang, J.C.L., and Sulkanen, M.E. 1987, *Astrophys. J.*,**315**, 504.

Lovelace, R.V.E., Berk, H.L., and Contopoulos, J. 1991, *Astrophys. J.*,to appear.

Lynden-Bell, D. 1969, Nature, **223**, 690.

Matsumoto, R., Horiuchi, T., Shibata, K., and Hanawa, T. 1988, *Pub. Astr. Soc. Japan*, **40**, 171.

Narayan, R., Goldreich, P., Goodman, J. 1987, *Monthly Notices Roy. Astron. Soc.*, **228**, 1.

Pringle, J.E. 1981, *Ann. Rev. Astron. Astrophys.*, **19**, 137.

Richtmyer, R.O., and Morton, K.W. 1967 *Difference Methods for Initial Value Problems* (2nd ed.; New York: Interscience), chap. 13.

Rubin, E., and Burstein, S.Z. 1967, *Comput. Phys.*, **2**, 178.

Sato, T., and Hayashi, T. 1979, *Phys. Fluids*, **22**, 1189.

Shakura, N.I., and Sunyaev, R.A. 1973, *Astron. Astrophys.*,**24**, 337.

Shibata, K. 1983, *Pub. Astr. Soc. Japan*,**35**, 263.

Shibata, K., and Uchida, Y. 1985, *Pub. Astr. Soc. Japan*,**37**, 31.

Shibata, K., Tajima, T., and Matsumoto, R. 1990, *Astrophys. J.*,**350**, 295.

Tajima, T., and Gilden, D. 1987, *Astrophys. J.*,**320**, 741.

Tajima, T. 1989, *Computational Plasma Physics* (Addison-Wesley, Redwood City, CA).

Uchida, Y., Shibata, K., and Sofue, Y. 1985, *Nature*,**317**, 699.

Umemura, S, Iki, K., Shibata, K., and Sofue, Y. 1988, *Pub. Astr. Soc. Japan*, **40**, 25.

Verbunt, F. 1981, *Space Sci. Rev.*, **32**, 379.

Figure capitons

Fig. 1 Numerical results for four different time steps, (a) the contour lines of B_z, (b) the density contours ($\log \rho$), (c) the velocity perturbation ($\delta V_x, \delta V_y$). Total illustrated area is (5×10) in the unit of h_0. The contour level step-width is 0.9 for (a) in the unit of linear scale and 0.2 for (b) in the unit of logarithmic scale. The scale VNh of the velocity vector is shown at the top of the figure in (c) in the unit of the isothermal speed of sound. Numbers in the lefthand side of each frame in (a) represent the time in units of the Keplerian period.

Fig. 2 The azimuthally averaged radial distributions of (a) the azimuthal component of velocity V_y, (b) the total pressure P_{tot}, (c) the thermal pressure p, (d) the magnetic pressure p_{mag}, (e) the density ρ, and (f) the α-parameter in the initial and final states.

Fig. 3 Time variations of magnetic (E_m), thermal (E_{th}), kinetic (E_k), gravitational (E_g) and total (E_{tot}) energies, where all energies are normalized to their initial values.

Fig. 4 Time dependence of the kinetic energy of the perturbations for different wavenumbers k of the initial perturbation as a function of $k^{1/2} \cdot t$.

Fig. 5 Time dependence of the kinetic energy of the perturbations for different plasma β of the initial magnetic field configuration. We show the cases $\beta_0 = 0.1, 1.0, 5.0$ and 10.0 with a grid size of $\Delta z = 0.1$, $\Delta y = 0.4$, and also the cases $\beta_0 = 0.2$ and 5.0 with a grid size of $\Delta z = 0.033$, $\Delta y = 0.4$.

Fig. 6 Time dependence of the kinetic energy of the perturbations for different shear rates q of the initial azimuthal velocity profile.

Fig. 7 Time variations of (a) the contour lines of B_z, (b) the density contours ($\log \rho$), (c) the velocity perturbation ($\delta V_x, \delta V_y$) for the case of a steady magnetic field at the inner boundary. Other remarks are the same as in Fig. 1.

Fig. 8 The azimuthally averaged radial distributions of (a) the azimuthal component of velocity V_y, (b) the total pressure P_{tot}, (c) the thermal pressure p, (d) the magnetic pressure p_{mag}, (e) the density ρ, and (f) the α-parameter at different timesteps for the case of a steady magnetic field at the inner boundary.

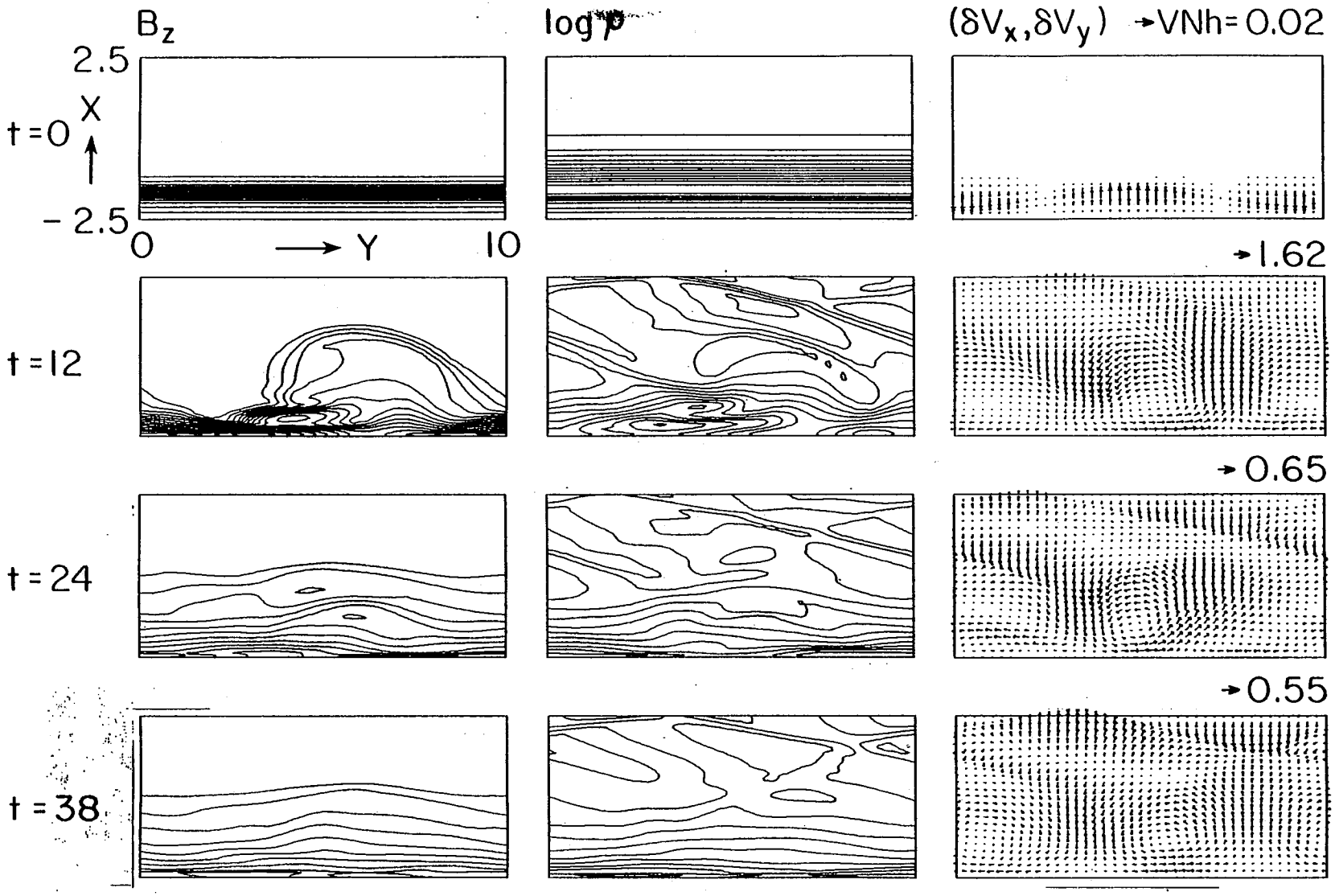
B_z
log ρ
$(\delta V_x, \delta V_y)$ →VNh= 0.02
2.5
X
t = 0
- 2.5
0
→ Y
10
→1.62
t = 12
→0.65
t = 24
→0.55
t = 38

Fig. 1

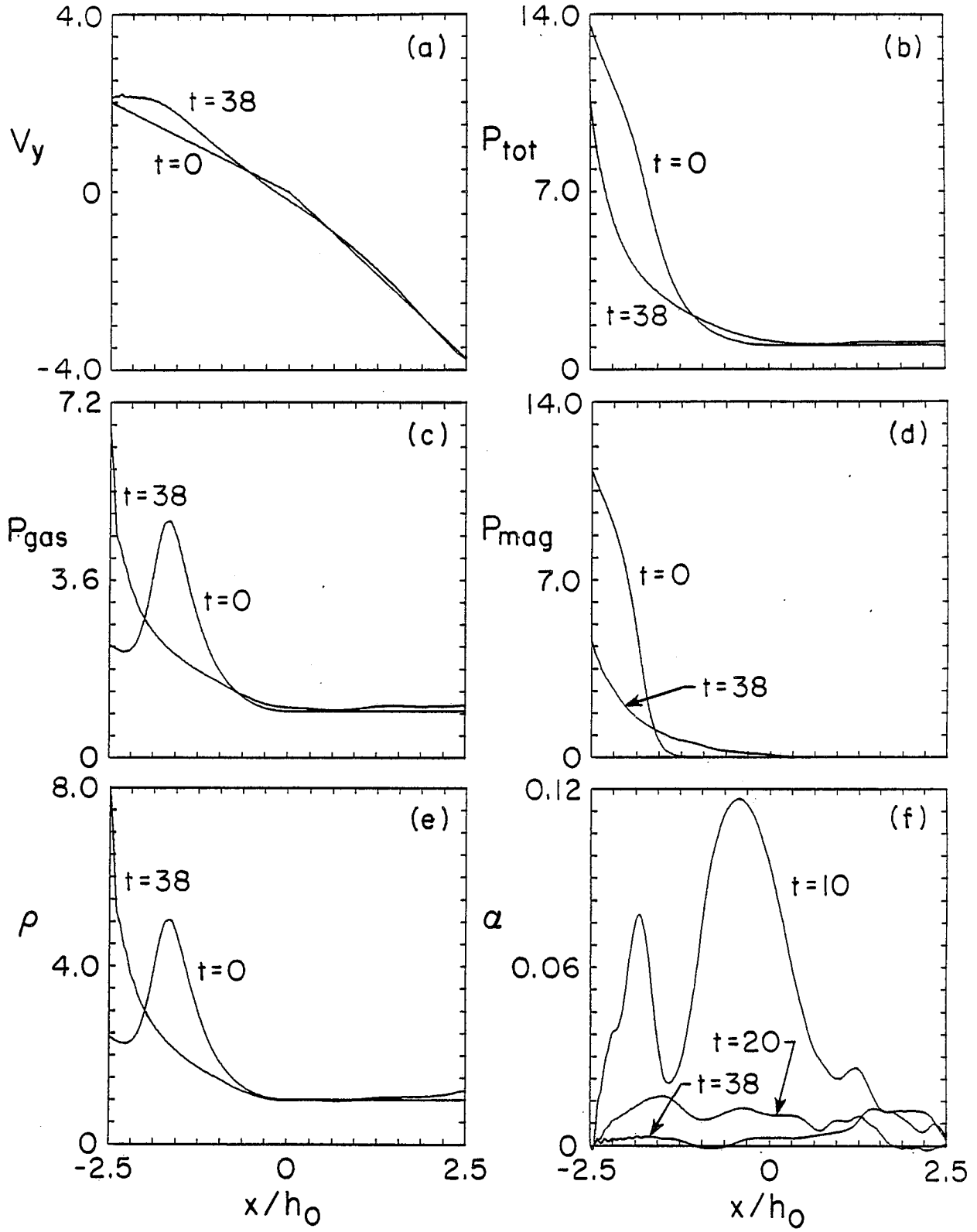
(a)
4.0
0
-4.0
V_y
t=38
t=0
(b)
14.0
7.0
0
P_{tot}
t=0
t=38
(c)
7.2
3.6
0
P_{gas}
t=38
t=0
(d)
14.0
7.0
0
P_{mag}
t=0
t=38
(e)
8.0
4.0
0
ρ
t=38
t=0
(f)
0.12
0.06
0
α
t=10
t=20
t=38
-2.5
0
2.5
x/h_0
-2.5
0
2.5
x/h_0

Fig. 2

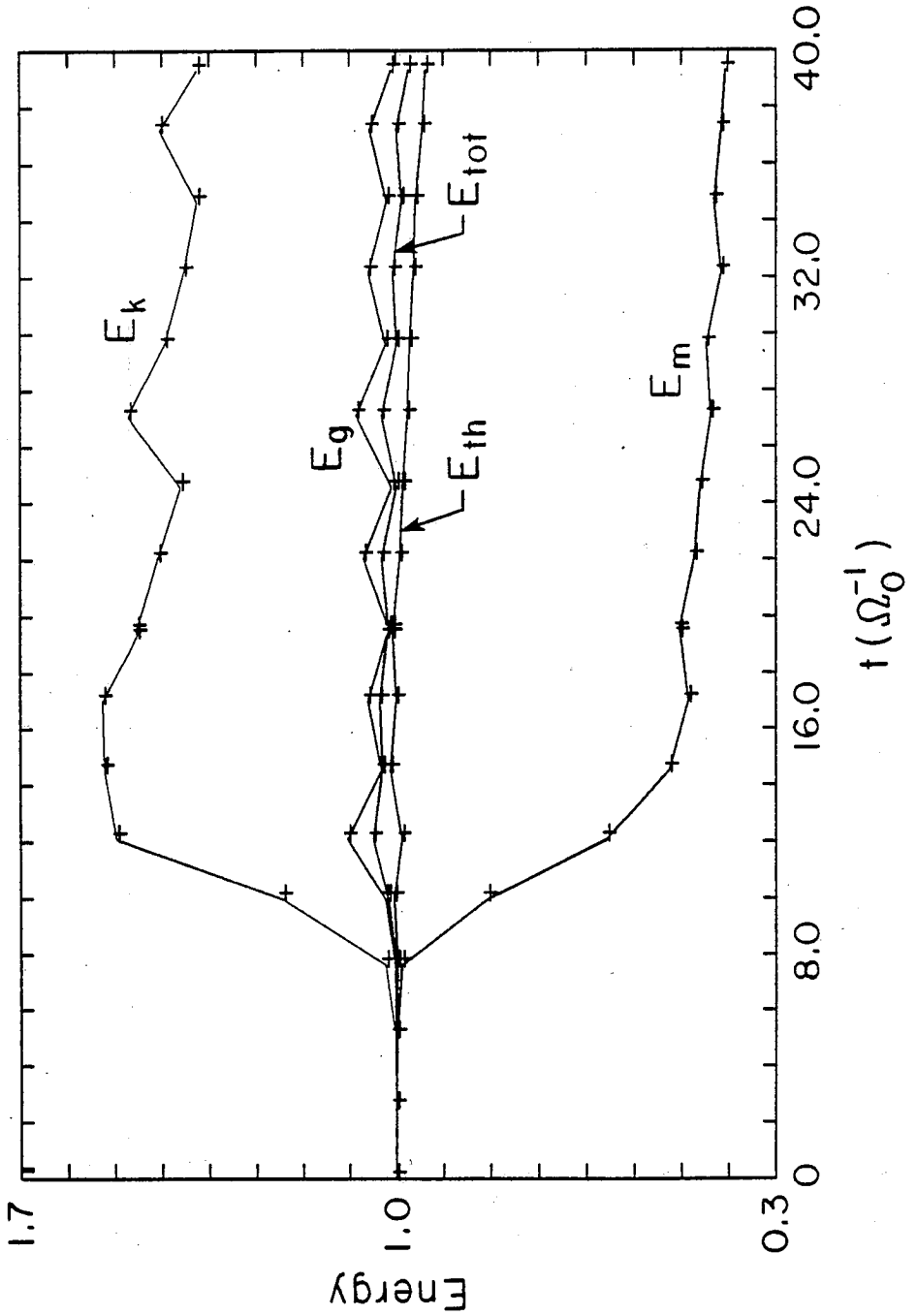

Fig. 3

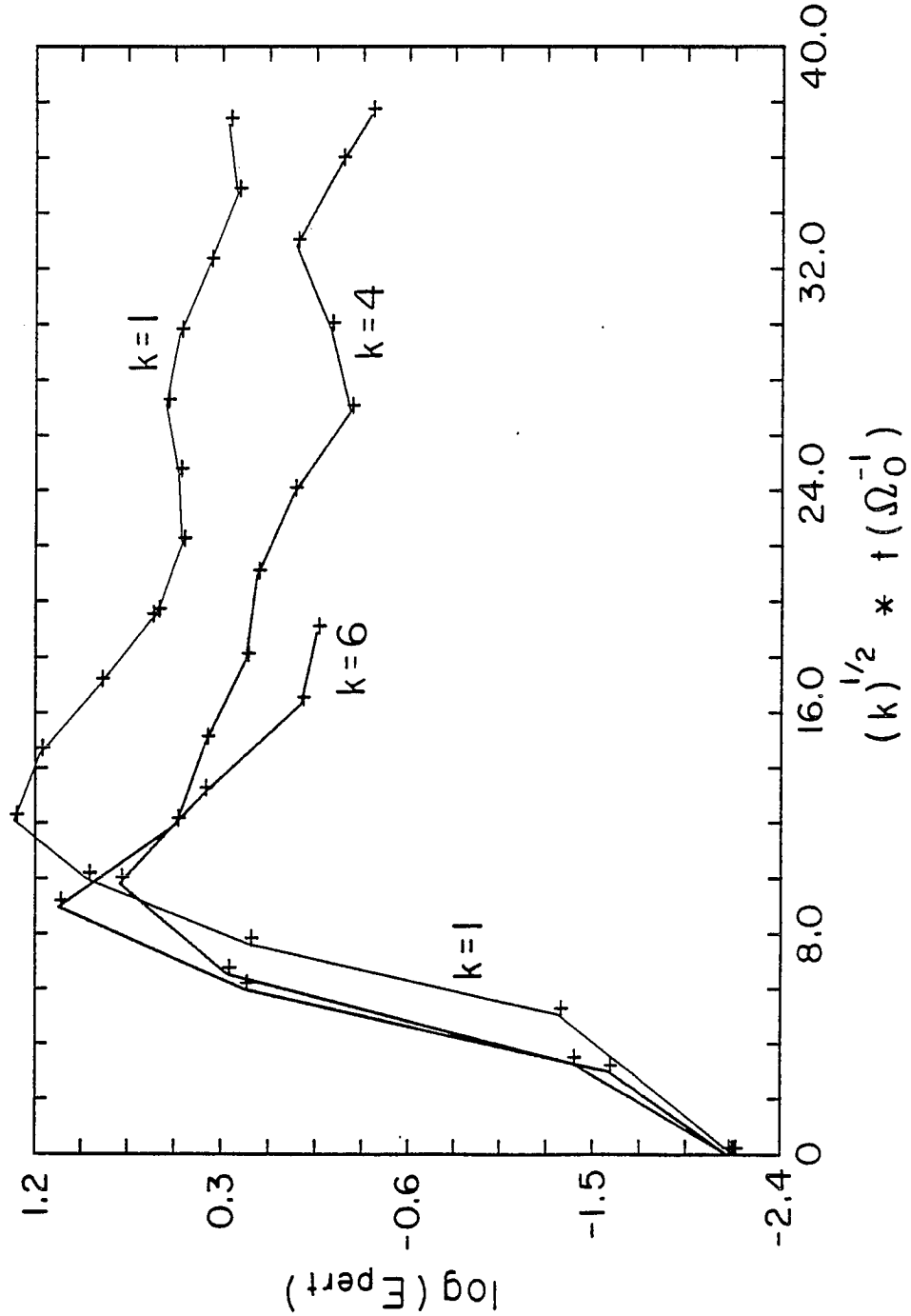

Fig. 4

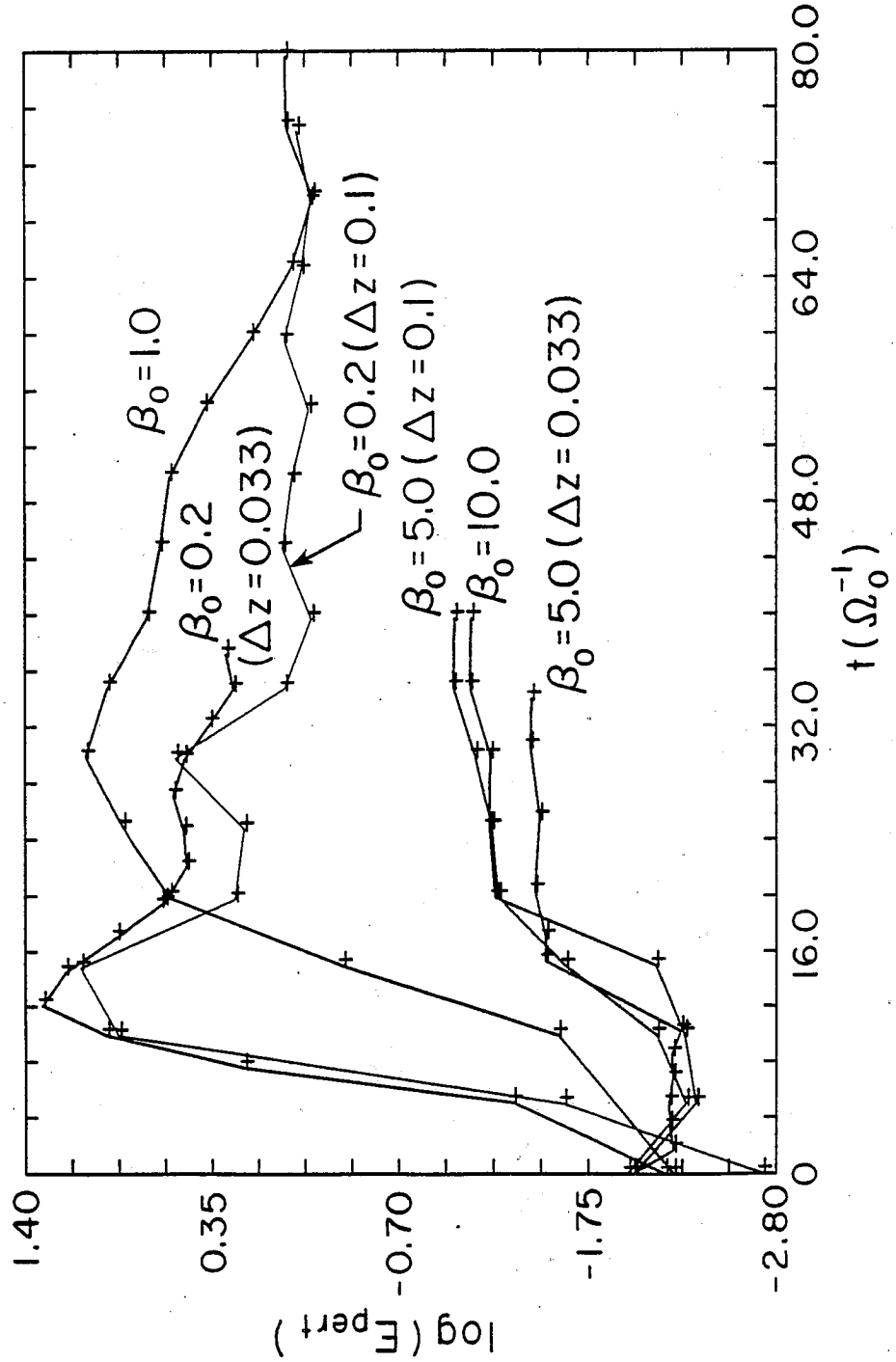
1.40
0.35
-0.70
-1.75
-2.80
0
16.0
32.0
48.0
64.0
80.0
log (E_pert)
t (Ω_o^-1)
β_o=1.0
β_o=0.2 (Δz=0.033)
β_o=0.2 (Δz=0.1)
β_o=5.0 (Δz=0.1)
β_o=10.0
β_o=5.0 (Δz=0.033)

Fig. 5

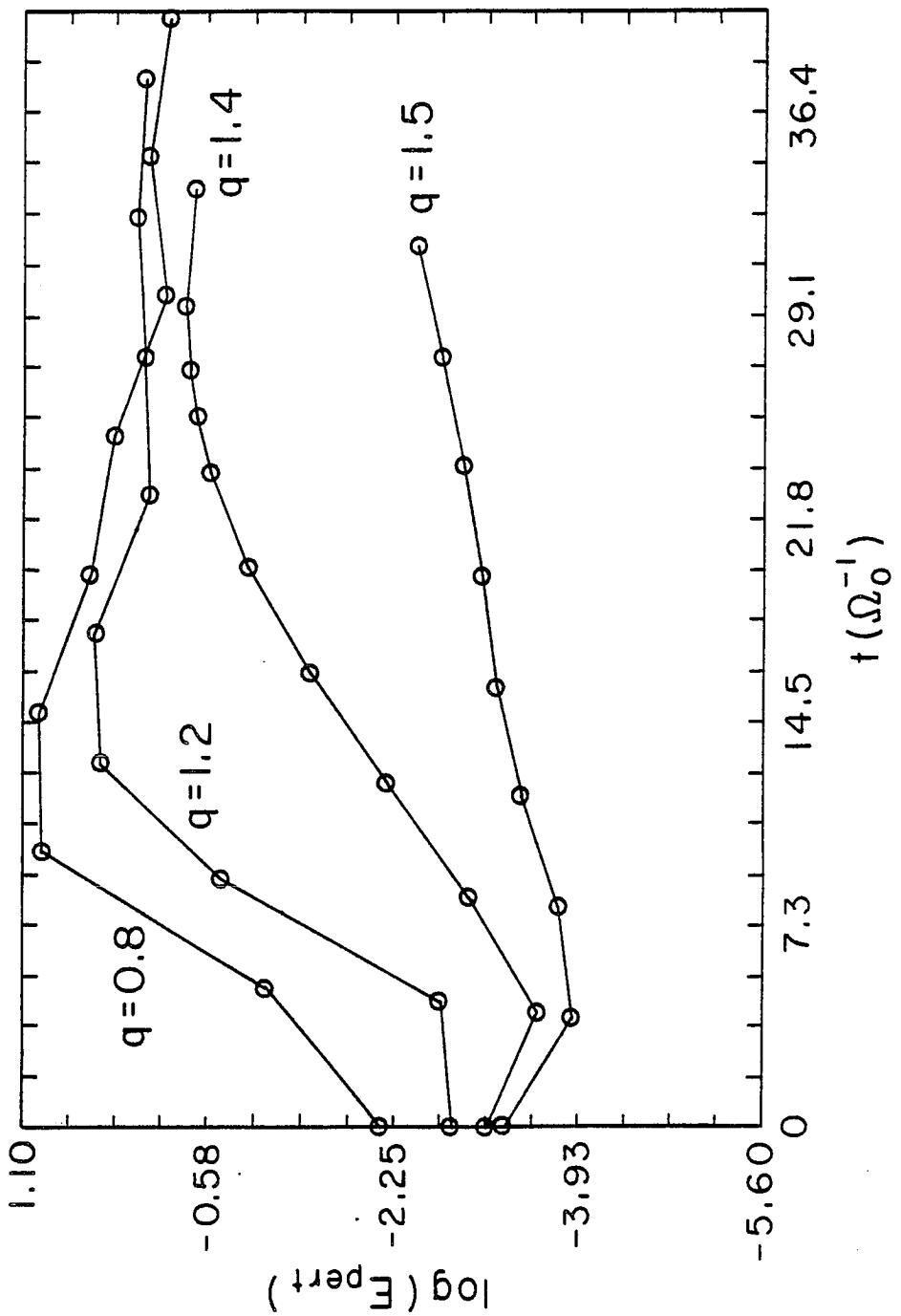
1.10
-0.58
-2.25
-3.93
-5.60
log (FT pert)
0
7.3
14.5
21.8
29.1
36.4
t (Ω_o^{-1})
q=0.8
q=1.2
q=1.4
q=1.5

Fig. 6

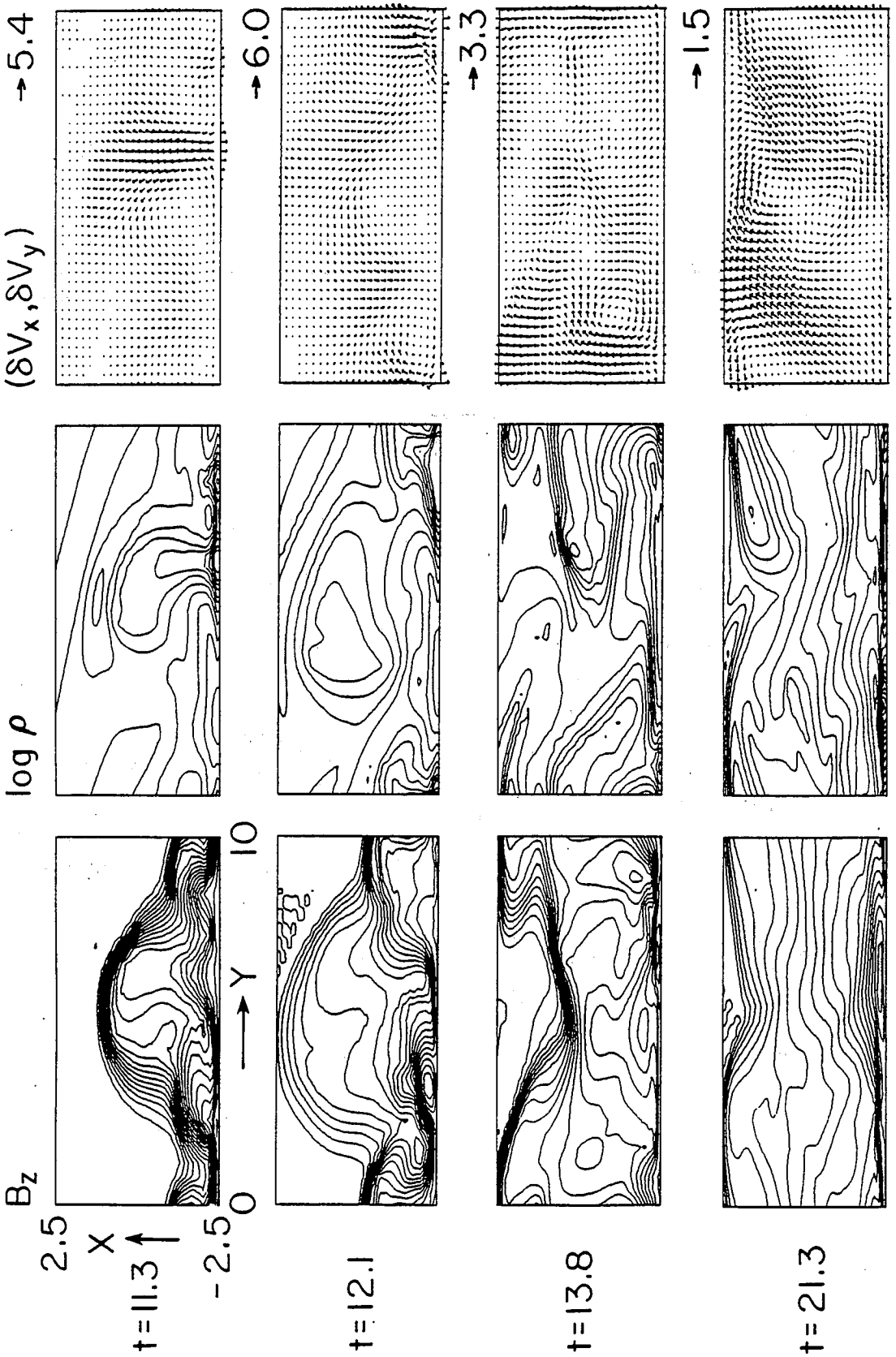
B_z
log ρ
$(\delta V_x, \delta V_y)$
→5.4
→6.0
→3.3
→1.5
2.5
X
-2.5
0
Y
10
t=11.3
t=12.1
t=13.8
t=21.3

Fig. 7

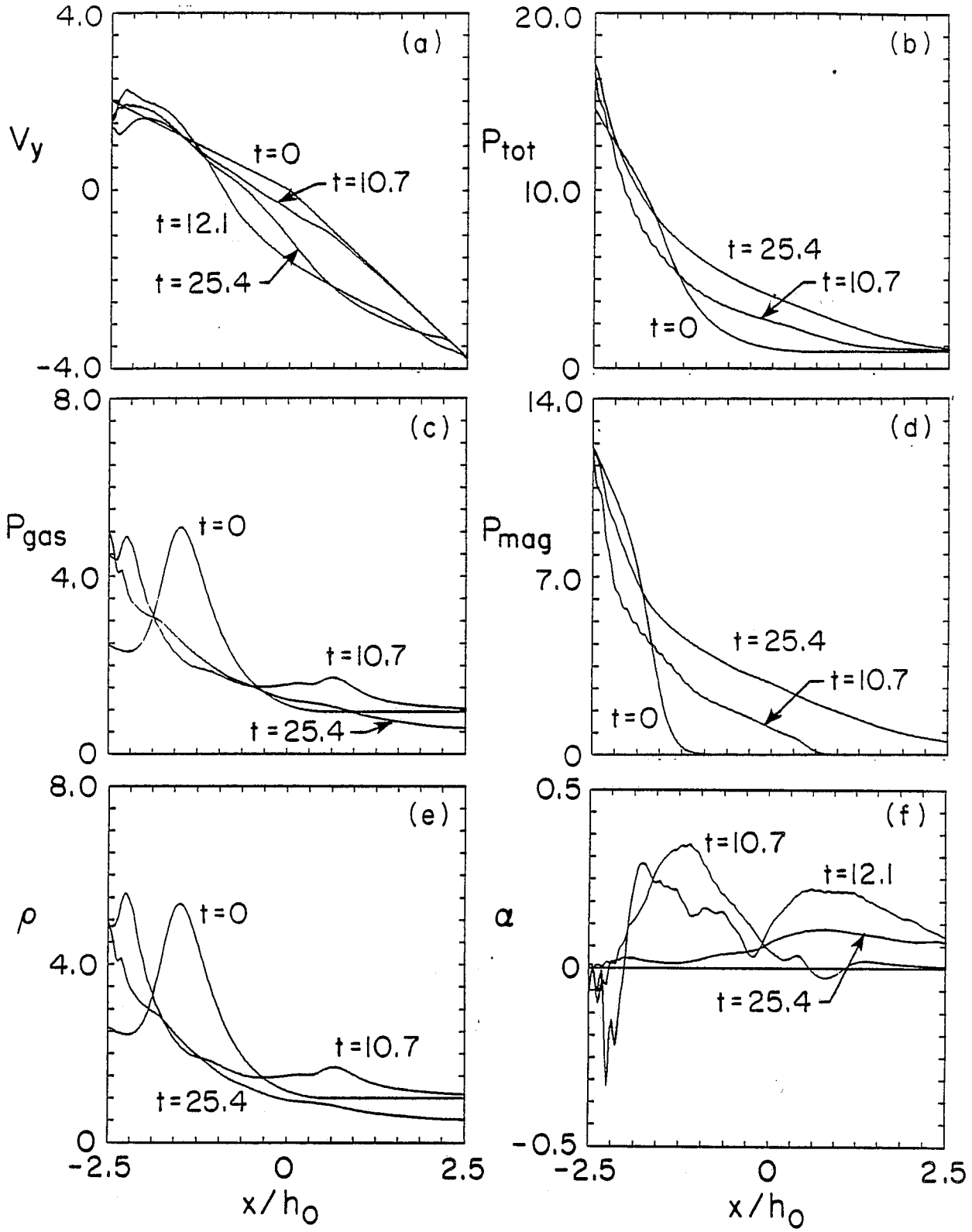
(a)
V_y
4.0
0
-4.0
t=0
t=10.7
t=12.1
t=25.4
(b)
P_{tot}
20.0
10.0
0
t=25.4
t=10.7
t=0
(c)
P_{gas}
8.0
4.0
0
t=0
t=10.7
t=25.4
(d)
P_{mag}
14.0
7.0
0
t=25.4
t=10.7
t=0
(e)
ρ
8.0
4.0
0
t=0
t=10.7
t=25.4
-2.5
0
2.5
x/h_0
(f)
α
0.5
0
-0.5
t=10.7
t=12.1
t=25.4
-2.5
0
2.5
x/h_0

Fig. 8